Hydration of Ferric Chloride and Nitrate in Aqueous Solutions:
Water-mediated Ion Pairing Revealed by Raman Spectroscopy

Journal:	*Physical Chemistry Chemical Physics*
Manuscript ID	CP-ART-03-2019-001392.R1
Article Type:	Paper
Date Submitted by the Author:	03-Jul-2019
Complete List of Authors:	Baumler, Stephen; The Ohio State University, Department of Chemistry and Biochemistry Hartt, V, William; The Ohio State University, Department of Chemistry and Biochemistry Allen, Heather; The Ohio State University, Department of Chemistry and Biochemistry

SCHOLARONE™
Manuscripts

Hydration of Ferric Chloride and Nitrate in Aqueous Solutions: Water-mediated Ion Pairing Revealed by Raman Spectroscopy

Stephen M. Baumler, William H. Hartt V, and Heather C. Allen*

Department of Chemistry & Biochemistry, The Ohio State University,

100 West 18th Avenue, Columbus, Ohio 43210, United States

Abstract

Iron is the most abundant transition metal in earth's crust and is important to proper functioning of many technological and natural processes. Despite the importance, a complete microscopic understanding of the hydration of ferric ions and water mediated ion pairing has not been realized. Hydrated Fe(III) is difficult to study due to the process of complexation to the anion and hydrolysis of the hydrating water molecules leading to a heterogeneous solution with diverse speciation. Here, ferric chloride and nitrate aqueous solutions are studied using polarized Raman spectroscopy as a function of concentration and referenced to their respective sodium salt or mineral acid. Perturbed water spectra (PWS) were generated using multivariate curve resolution-alternating least squares (MCR-ALS) to show the residual spectral response uniquely attributable to the hydration of ferric speciation. The hydrogen bonding network associated with the hydrating water molecules in ferric chloride solutions are found to be more similar to hydrochloric acid solutions, whereas in ferric nitrate solutions, the network behaves more similar to sodium nitrate, despite increased acidity. Thus, in the $FeNO_3$ and $FeCl_3$ solutions, ion pairing and coordination, respectively, are significantly influencing the hydration spectra signature. These results further reveal concentration dependent changes to the hydrogen bonding network, hydrating water symmetry, and changes to the relative abundance of solvent shared ion pairs that are governed primarily by the ferric salt identity.

Introduction

Iron is one of the most abundant transition metals found on earth and has an immense impact on many physical, chemical, and biological processes. The focus of many research efforts on solvated iron species has been dominated by the oxide-hydroxide materials and molecular hydrolysis species present at low concentration and near neutral pH. Species present under these conditions have direct relevance to the corrosion of iron alloys, geochemical weathering of iron containing minerals, cosmo- and extra-terrestrial chemistry,[1, 2] polluted water remediation, and atmospheric and oceanic chemistry.[3-6]

Despite the many years of continued research, a complete understanding of the hydration of ferric ions has not been fully understood. The complexity due to the diverse speciation created upon dissolution results in an aqueous environment containing a complex mixture of ionic species that are both pH and concentration dependent. Iron complexes containing covalently bound inorganic ligands, such as chloride, nitrate, and sulfate, are often overlooked from the aqueous solvation models due to oversimplification or difficulty in studying their transient nature. Additionally, both kinetic and thermodynamic equilibria drive the formation of insoluble colloidal iron oxides and oxide-hydroxides. Given the complexity resulting from the dissolution of a single molecular species, it is not surprising that many models are oversimplified.

In the solid phase, the crystal structure of ferric chloride hexahydrate was first observed by Lind as trans-$[Fe(H_2O)_4Cl_2]^+$ octahedral complexes containing a solvent shared chloride ion pair with Fe-Cl (2.30Å), Fe-O (2.07Å), and Cl-O (3.12Å and 3.06Å) bond distances.[7] Distances between two neighboring cationic iron complexes suggest solvent shared ion pairs may exist at concentrations close to that of the hexahydrate.[7] In contrast, $FeCl_3 \cdot 2\frac{1}{2}H_2O$ was observed by Szymanski as distorted cis-$[Fe(H_2O)_4Cl_2]^+$ and tetrahedral-$[FeCl_4^-]$ with Fe-Cl (2.17-2.25Å), Fe-O

(2.00-2.12Å) bond distances.[8] Observed bond length and angle differences between the two hydrates were attributed to changes in the hydrogen bonding structure between ferric complexes and the associated hydrating waters.

Ferric nitrate nonahydrate $[Fe(H_2O)_6](NO_3)_3 \cdot 3H_2O$ in the solid state was observed to have similar Fe-O bond distances (1.99±0.14Å) to the chloro- equivalent, however no direct contact between nitrate and iron was observed.[9] The octahedral complexes exist primarily as hexaaquoiron $[Fe(H_2O)_6]^{3+}$ with the nitrate anion found in close proximity to the first hydration shell. Dehydration of the nonahydrate yields iron nitrate complexes of $[Fe(H_2O)_5NO_3]^{2+}$ and $[Fe(H_2O)_3(NO_3)_2]^+$.[10] The degree of covalency between the nitrate and metal center is not evidentially clear from the literature.

The structure of ferric chloride and nitrate complexes in aqueous solutions have also been examined by a range of X-ray diffraction[11, 12], X-ray scattering[13, 14], and neutron scattering[15-17] techniques. The result of these studies has generated debate on the existence of higher order chloro- , dimer and trimer, and oxo- and hydroxo- bridged ferric complexes. Recently, EXAFS studies by Persson assert the dominance of the trans-$[Fe(H_2O)_4Cl_2]^+$ complex even after additional chloride concentrations up to 1 mol/L are added.[14] Despite success in defining the properties of waters hydrating the ferric ions, longer range structure and interaction characterization is difficult for X-ray and neutron techniques due to decreased structural ordering in successive hydration shells.[18-20]

Efforts to understand the structure of ferric species in aqueous solutions and hydrated melts have also been studied using Raman[21-26] and FTIR vibrational spectroscopy[27, 28]. Early work by Sharma et. al. provided spectroscopic evidence in broad agreement with the X-ray studies, discussed previously. In hexahydrated melts, the cis-$[Fe(H_2O)_4Cl_2]^+$ and tetrahedral-$[FeCl_4^-]$

species are most prevalent.[22] In contrast to the studies by Schmidt et. al., Sharma observed iron nitrate complexation in the nonahydrate melts.[10, 23] More recently, THz spectroscopy has been used by Havenith and co-workers to examine the structure and interactions of iron chloro- and hexacyano- complex ion pairs on the librational vibrations of water.[29, 30]

One of two techniques found in the literature to directly examine the perturbation to the hydrogen bonding network of water due to solute solvation is referred to as double difference spectroscopy pioneered by Lindgren and advanced by Stangret.[31-34] The technique first requires vibrational difference spectra between salt solutions to pure water and ~10% HDO solutions. Difference between the pure water and HDO difference spectra reveal hydration shell OD stretches.[32] Ben-Amotz and co-workers have developed a second technique termed self-modeling curve resolution (SMCR) on high-quality Raman spectra to deconstruct the individual spectral contributions of hydronium and counterions to better understand solvation shell structure.[35-37] Similar application of SMCR on attenuated total reflection infrared spectroscopy (ATR-FTIR) spectra has led to observation of the solvation structure around tert-butanol.[38] In contrast to double difference spectroscopy, SMCR does not require isotopically labeled spectra. Instead, this method utilizes a modified method of multivariate curve resolution alternating least squares (MCR-ALS) statistical analysis to deconvolute the perturbed spectra from the solvent spectral response.[36]

Here, we examine aqueous ferric chloride and ferric nitrate salt solutions, under intrinsically acidic (pH<5) conditions, and over a concentration series from 0 - 0.6 m using multivariate curve resolution alternating least squares on polarized Raman spectra. The perturbed water spectra (**PWS**) observed through multivariate curve resolution alternating least squares analysis reveal water restructuring. Changes to symmetry around the ferric ions is driven by hydration and complexation and for ferric chloride, these changes are affected by the presence of

several ferric chloride species of varying relative abundance. Anion type and increased hydronium concentration play a role in changes to the hydrogen bond network of hydrating water molecules as observed by comparison to aqueous solution spectra containing only mineral acids (HCl and HNO_3) and salts (NaCl and $NaNO_3$).

Experimental Section

Sample preparation. Ferric samples were prepared by dissolving weighed amounts of $FeCl_3 \cdot 6H_2O$ or $Fe(NO_3)_3 \cdot 9H_2O$ in water from a MilliQ source (18.2MΩ) to a total concentration of 1m. The 1m stock solutions were used for subsequent dilutions to the desired molality. The mineral acid samples containing HCl or HNO_3 and salt solutions containing NaCl or $NaNO_3$ were prepared similarly. All salts were purchased from Acros Organics (>99%+ purity), acids from Fisher Scientific (TraceMetal^{TM} grade), and used as received.

Raman spectroscopy. Polarized Raman spectra were collected using a home-built polarized Raman spectrometer with a diode pumped 532nm CW laser containing built-in laser line (+/- 0.5nm) and polarization (>100:1 V) filters (CrystaLaser). Excitation was directly coupled to a custom-built fiber optic polarized Raman probe system (InPhotonics) allowing *ca.* 235 mW power at the sample with a spectral range of 90-4200 cm^{-1} and output parallel-polarized (V) and perpendicular-polarized (H) scattered light to two independent FC fiber-optic terminated ports. The two polarized output ports were fiber coupled directly to a spectrograph with a 600 g/mm grating; wavelength calibrated to He:Ne emission lines (IsoPlane 320, Princeton Instruments) and detection from a liquid nitrogen cooled CCD detector (Pylon, 1340 x 400 pixel, Princeton Instruments). Coupling of each 200 μm core fiber directly to the spectrograph allowed simultaneous collection of the perpendicular (HV) and parallel (VV) polarized spectra (Figure

S1A). Experiments were performed at a room temperature of ~20 °C. Spectra reproducibility point to solution tolerance to the laser power as sample degradation was not observed. Spectra were collected by signal averaging 25 spectra each with a 0.4s integration time.

Spectral Post-processing. Background was removed by subtracting the spectrum obtained for an empty sample vial. A depolarization correction factor *(G = 0.54)* was calculated using the depolarization ratio ρ known for water in the literature to within 0.02 (Eq. 1).[39-41]

$$\rho = \frac{GI_{\perp}}{I_{\|}} \tag{2}$$

Isotropic and anisotropic spectra were calculated from the frequency dependent parallel $I_{\|}$ and perpendicular $I_{\perp}$ Raman intensities by Eqs. 2-3.[42] Unpolarized spectra were calculated by summation of the parallel and perpendicular corrected intensity.

$$Isotropic = I_{\|} - \left(4/3\right)GI_{\perp} \tag{3}$$

$$Anisotropic = \left(4/3\right)GI_{\perp} \tag{4}$$

MCR-ALS GUI 2.0 toolbox for Matlab was used for calculation of the nonzero minimum area differences between two spectra.[43, 44] Concentrations of each solute were used as initial estimates for the two component concentration matrix. Non-negativity constraints were applied using the fast non-negative least squares method (FNNLS). Convergence, defined as a change in lack-of-fit between consecutive iterations <0.1%, for the multivariate curve resolution alternating least squares algorithm was achieved for all analyzed spectra (details for the MCR-ALS method can be found in the Supplementary Information).

Results & Discussion

Terminology. Diverse terminology is in the literature to describe various molecular complexes and environments that exist when hydrating an ionic solute stemming from language more common to the physical chemistry ion pairing versus the inorganic coordination chemistry literature. Here we adopt the physical chemistry language as it more simply describes our Raman spectral observables. Thus, water molecules immediately surrounding ions are referred herein as first solvation shell water molecules, although they may be covalently bonded or "coordinated". Successive water molecules in the next layer surrounding that of the first solvation shell water molecules are referred to as the second hydration shell water molecules, and so on. Association of an anion with the ferric ion exists with varying hydration levels. Also consistent with the physical chemistry ion pairing language, direct contact between anion and cation are termed contact ion pairs. Anions and cations mediated by water molecules in the 1st hydration shell, are termed "solvent shared ion pairs". Any anion-cation ion pair that are separated by 2 water molecules are termed "solvent separated ion pairs". The hydrogen bonding structure of water due to the presence of ion pairing types of varying relative abundance are the focus of this study.

Speciation of Fe(III). The dissolution of Fe(III) yields diverse speciation due to hydrolysis of the hydrating water and association with counter anion(s). Hydrating water molecules of Fe(III) undergo hydrolysis yielding a series of pH dependent Fe(III) hydrolysis species $[Fe(H_2O)_6]^{3+}$, $[Fe(H_2O)_5(OH)]^{2+}$, $[Fe(H_2O)_4(OH)_2]^+$, and $[Fe(H_2O)_3(OH)_3]$, where these species contain both neutral water molecules and hydroxide ions.[45-48] At lower pH, the presence of dimer $[Fe_2(H_2O)_8(OH)_2]^{4+}$ and trimer $[Fe_3(H_2O)_{10}(OH)_4]^{5+}$ species have been observed.[45, 48-51]

Hydrolytic polymerization of the hydrated species to the most thermodynamically stable form of iron oxide-hydroxides consequentially increases the complexity of the solute-solvent environment as the kinetically driven process results in changes to the relative abundance in a solution over

time.[52] The thermodynamic formation constants at room temperature for the ferric hydrolysis, and

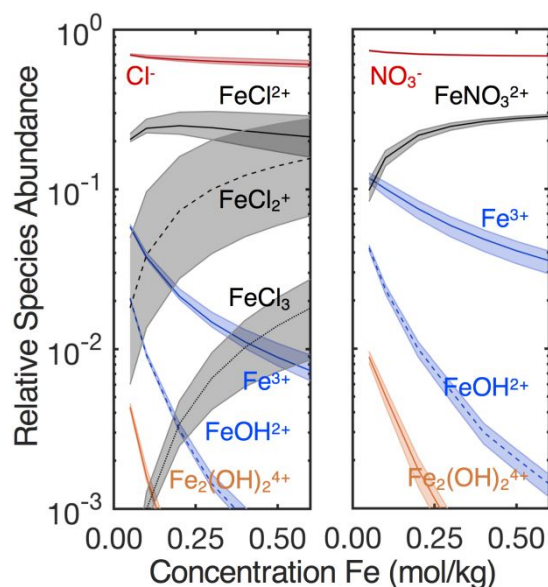chloro- and nitrate species are shown in Table S2.

FIGURE 1 HERE.

Figure 1: *Relative abundance (log scale) of ferric chloride (left) and ferric nitrate (right) species present at thermodynamic equilibrium as a function of total ferric ion concentration, truncated at $<10^{-3}$ relative abundance and labeled without primary shell waters for clarity. Shaded errors represent ± 1σ calculated from the literature values. (Details for the calculation of the relative species abundance can be found in the Supplementary Information S5.)*

Figure 1 shows the accepted relative species abundance of nitrate and chloride iron salts at thermodynamic equilibrium. Hydrolysis and complexation contribute to pH and ferric ion concentration dependent solution heterogeneity. At concentrations greater than $>10^{-1}$ m Fe(III), the most abundant species are ferric complexes containing the associated anions (Cl^- or NO_3^-). In the presence of chloride, the covalently bound chloride complexes $[Fe(H_2O)_5Cl]^{2+}$, $[Fe(H_2O)_4Cl_2]^+$, and $[Fe(H_2O)_2Cl_3]$ dominate in relative abundance.[53-60] A singular ferric nitrate complex

$[Fe(H_2O)_6NO_3]^{2+}$, without defined covalency, has been suggested to exist at thermodynamic equilibrium, although direct spectroscopic evidence is lacking.[61-64]

The ferric nitrate solutions exhibit a constant relative abundance of $[Fe(H_2O)_6NO_3]^{2+}$ in competitive equilibrium with hydrolysis species throughout the concentration ranges measured.[9, 17, 63] In contrast, the ferric chloride solutions exhibit changes in the ranking order of predominant species over the concentrations measured. The $[Fe(H_2O)_4Cl_2]^+$ complex is expected to be the most abundant at concentrations greater than ~0.4 m. At higher chloride concentrations ~0.5m, $[Fe(H_2O)_2Cl_3]$ surpasses $[Fe(H_2O)_6]^{3+}$ in relative abundance. The formation of $[Fe(H_2O)_4Cl_2]^+$ with $[FeCl_4]^-$ as a contact ion pair has been observed in hydrated melts of ferric chloride.[65-67]

As one expects, increasing the concentration of solute leads to a lower relative ratio of bulk-like water molecules to hydration water molecules (Table S1). To better understand the spectral features present from the hydration shell water molecules, ferric chloride and ferric nitrate were first dissolved at increasing concentrations in water (0-0.6m) and perturbations to the water spectral region were determined using MCR-ALS. It is important to note that application of MCR-ALS reflects the non-zero minimum area difference between two spectra; essentially, these can be viewed, albeit as an oversimplifying interpretation, as the absolute value of difference spectra. Recent work by Roke and co-workers has shown that solvation of electrolytes results in orientational ordering of the water dipole and disruption to the hydrogen bonding network into the third hydration shell.[68, 69] The MCR-ALS spectra, specifically the PWS, presented here can then be viewed as a convolution of both first and second hydration shell water spectra.

Ferric chloride hydration effects. Figure 2 shows unpolarized Raman spectra (solid blue lines) and the PWS (red dash-dot lines, multiplied by 2X) for 1.5m NaCl, 1.5m HCl, and 0.5m

FeCl$_3$ solutions (homologous spectra for ferric nitrate are shown in Figure S3) relative to the pure
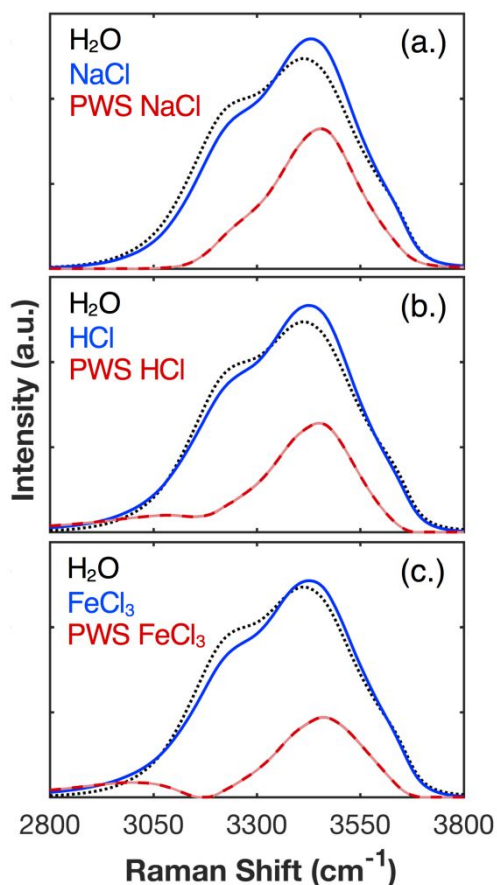
bulk water spectrum (dotted black line).

FIGURE 2 HERE

Figure 2: *Unpolarized Raman spectra (solid lines) of (a.). 1.5m NaCl, (b.) 1.5m HCl,*
*and (c.) 0.5m FeCl$_3$. Perturbed water spectra (**PWS**) are shown in red (dash-dot are*
amplified 2X for clarity), and pure water spectrum in black (dot).

Changes to peak intensity, peak full width at half max (FWHM), and peak frequency, are

all indicators of changes to the hydration environment (Table 1). We begin by discussing the

influence of the anion on the unpolarized Raman spectra. Hydration of halide-containing

electrolytes results in an increased peak intensity of the 3420 cm^{-1} band compared to pure water

(Figure 2). Enhancement of the Raman cross section (Raman transition moment) of this 3420 cm^{-1}

band is due to changes to both low energy charge transfer and changes to the electric field between

the anion and hydrating water molecules.[70, 71]

TABLE 1 HERE

Table 1: Peak frequency at max (ω), FWHM (σ), intensity at maximum, and relative area of PWS (Σ)

Solution	ω (cm^{-1})	σ (cm^{-1})	Intensity (a.u.)	Σ (%)[1.]
NaCl	3454 ± 1	246 ± 0(.2)	1.64 ± 0.01	21.8 ± 0.1
HCl	3448 ± 2	237 ± 1	1.28 ± 0.01	18.3 ± 0.2
FeCl$_3$	3462 ± 2	243 ± 1	0.94 ± 0.01	13.8 ± 0.1
NaNO$_3$	3472 ± 3	302 ± 1	1.18 ± 0.01	18.3 ± 0.2
HNO$_3$	3508 ± 3	237 ± 1	0.85 ± 0.01	14.2 ± 0.1
Fe(NO$_3$)$_3$	3505 ± 0	258 ± 1	0.87 ± 0.02	14.4 ± 0.3

[1.] Relative areas were calculated as the integrated area of the respective perturbed water spectrum divided by the area of the unpolarized salt (or acid) spectrum from 2500-3880 cm^{-1}. Values representative at a concentration of 0.5 m and errors represent ± 1σ for the averaged spectra of samples measured in triplicate.

FWHM of the perturbed water spectra has been found to correlate to the distribution of

electric field strengths experienced by the hydrating waters.[37, 71] As shown in Table 1, for the

solutions measured here, the PWS FWHM follows a general trend of non-iron salt > iron salt >

acid. The ferric ion salt and sodium salts spectral peak at ~3450 cm^{-1} is broadened relative to the

acid.   Given that the PWS FWHM can be correlated to the distribution of electric fields

experienced by hydrating water molecules, one might expect the degree of dissociation, or

distribution of ion pairing types, might also correlate to this effect.[72] NaNO$_3$ PWS FWHM (γ:

0.84, 1.5 m)[73, 74] are on average broader (by ~60 cm^{-1}) than NaCl (γ: 0.66, 1.5 m)[75, 76], and are

more dissociated as characterized by the solution activity coefficient.[77]   Note that activity

coefficients are correlated to ion-ion and ion-water interactions and thus association in solution,

which then may indeed be correlated to bandwidth of the OH stretch region, indicative of addition of varying hydration environments. However, broadening cannot be explained by this phenomena alone. HNO_3 (pKa: -1.4, γ: 0.76, 1.5 m)[78-80] and $NaNO_3$ (γ: 0.84, 1.5 m) solutions have similar activity coefficients; however, the difference in PWS FWHM is ~35 cm^{-1} whereas HCl (pKa: -7, γ: 0.90, 1.5 m)[81-83] and NaCl (γ: 0.66, 1.5 m) have a difference of ~10 cm^{-1}. The observed inconsistency between FWHM and activity coefficient suggests additional spectral contribution from water molecules specifically unique to the anionic identity in these solutions, sensitivity to the hydrating environment of the cations (sodium or ferric), or an enhanced electric field effect from solvent shared and solvent separated ion pairs.

Also revealed in Table 1, blue-shifting of the ferric chloride (~6 cm^{-1}) and ferric nitrate (~35 cm^{-1}) maximum band relative to their analogous monovalent salt is observed. This may be attributed to water molecules in the 1st and 2nd hydration shell of ions. Geissler and coworkers demonstrated that the strong electrostatic forces exerted by ions and observable by Raman spectroscopy are most strongly felt by the 1st and to a much lesser extent, the 2nd hydration shell water molecules.[71] The broad asymmetric band present in the PWS for the acid (Figure 2b and S3b) and ferric salt (also an acid, Figure 2c and S3c) at frequencies lower than 3220 cm^{-1} arises from a proton continuum resonance.[84, 85]

Similar to difference spectral subtraction methods, MCR-ALS PWS can be effectively used to remove the large anionic contribution by choosing the corresponding sodium salt or mineral acid as the 'solvent' contribution to be removed from the ferric solution spectrum such that the ferric species is the 'solute-of-interest'. (Again, note that

these spectra where the solvent is defined uniquely, can be interpreted similarly to the

absolute value of difference spectra.) Spectral differences between the ferric solutions

and salt or acid solution structure can then reveal the cationic or ion pair contribution to

the polarized Raman water bands more robustly as compared to removing the pure water

contribution from bulk water spectra as was done in Figure 2. Therefore, in Figure 3, we

show the unpolarized Raman PWS of the iron salts when the 'solvent' contribution is chosen to be

the corresponding salt or acid. Thus, choosing to remove the acid spectral contribution reveals

water structure that is unique to the contribution by the (1) ferric hydrolysis species, (2) hexaaquo-

ferric ions, and (3) any changes to the ion pair distribution with respect to the acid. In another

view, when the 'solvent' is chosen as the salt, water molecules unique to changes to the same 3

species/factors with respect to the salt are revealed. In this way, water molecules and electric field

contributions arising from ferric salt ion pairing are further elucidated.
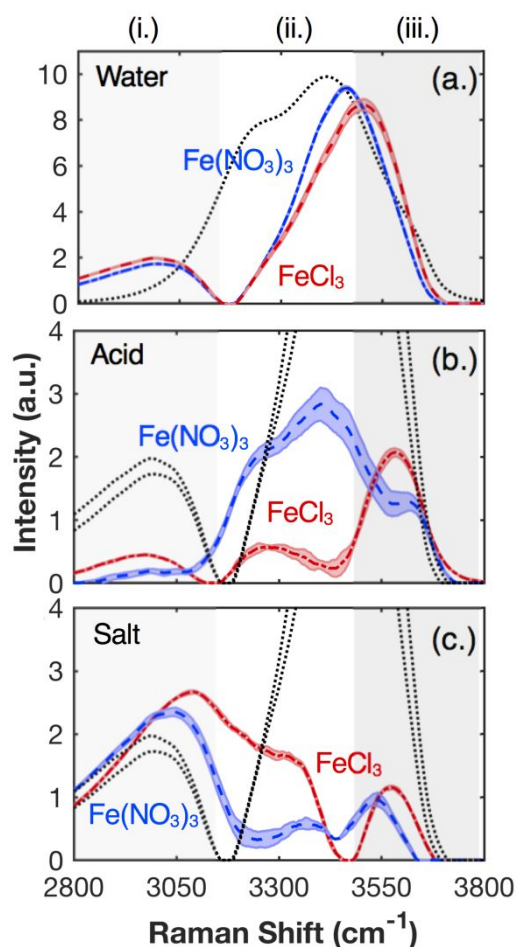
FIGURE 3 HERE

Figure 3: Unpolarized PWS of the ferric salt solutions. (a.)PWS of iron solutions with water as 'solvent.' Water is reduced by 0.2 times and shown for reference (black dotted line). (b.) PWS of iron solutions with acid as 'solvent.' (c.) PWS of iron solutions with salt as 'solvent.' PWS when water is solvent are shown in (b.) and (c.) for reference (black dotted lines). FeCl$_3$ (0.5 m, red dash-dot) and Fe(NO$_3$)$_3$ (0.5 m, blue dash). Iron solutions were referenced to their respective anion at 3 times concentration (1.5 m) for both acid and salt analysis. Regions of interest (i.-iii.) are discussed in the text.

There are three regions of interest in the acid and salt contribution PWS (Figure 3). In all three regions, there are only slight differences in Figure 3a of the water-removed spectra, yet there is significant blue shift observed for FeCl$_3$ versus the Fe(NO$_3$)$_3$ solution spectra. Figures 3b and

3c reveal differences more obviously for the associated acid-removed and salt-removed spectra (PWS) for both salts.

The intensity of the first region (i.) <3200 cm^{-1} is suppressed in the acid-removed (FeCl$_3$-HCl and Fe(NO$_3$)$_3$-HNO$_3$) PWS (Figure 3b) and enhanced in the salt-removed (FeCl$_3$-NaCl and Fe(NO$_3$)$_3$-NaNO$_3$) PWS (Figure 3c) due to contribution from the proton continuum arising from iron hydrolysis. There still exists a nonzero contribution to the proton continuum region in FeCl$_3$-HCl due either to a cationic contribution other than the proton continuum, water molecules associated to an ion pair, or perturbation to the proton continuum different than what was evident from the corresponding acid spectrum (that was removed). The concentration of protons in the ferric chloride solutions is ~20x less than the HCl solution (from simply calculated the relative number of protons from the 2 solutions), suggesting that the remaining contribution is from strongly hydrogen bonded water molecules that are hydrating Fe(III) ions. Similarly, other multivalent cations have been previously shown to contribute peak intensity of SMCR spectra in this region.[35]

The second region (ii) 3200-3500 cm^{-1} reveals successful suppression of the chloride hydration shell contribution in both FeCl$_3$-HCl and FeCl$_3$-NaCl PWS, as one would expect. The acid referenced Fe(NO$_3$)$_3$-HNO$_3$ PWS shows increased intensity in region (ii) compared to FeCl$_3$-HCl. For the two ferric salts, the hydrogen bonding network of water in the ferric chloride solutions is more similar to HCl, whereas the hydrogen bonding network in ferric nitrate solutions is more similar to NaNO$_3$.

Similarity between the ferric chloride solutions and HCl as evidenced by the HCl-removed FeCl$_3$-HCl PWS suggests that the chloride hydrating-water spectral contribution in the FeCl$_3$

solution is structurally similar to the acid's Cl⁻. In contrast, the increased intensity in region (ii) for the acid-removed $Fe(NO_3)_3$-HNO_3 and decreased intensity in the salt-removed $Fe(NO_3)_3$-$NaNO_3$ PWS is consistent with hydration more similar to the $NaNO_3$ solution, despite higher acid content for $Fe(NO_3)_3$ solutions when compared to $FeCl_3$ solutions. For both iron salts, the remaining contributions present in the second (ii) and in the third regions (iii) >3500 cm⁻¹ are assigned to strong and weak-hydrogen bonded water molecules as influenced by the ferric ion hydration, respectively.

The spectral deconvolution as shown in Figure 3 reveals strong evidence that the hydrating water molecules are sensitive to much more than the acidity of the ferric ions and the hydration of the counter ion. We further highlight that ion pairing interactions are the obvious missing link to understanding the spectral residual intensity left in the MCR-ALS / PWS analysis, albeit assigning the residual intensities to water molecules specifically in solvent shared or solvent separated ion pairs needs further detailed analysis, and likely theoretical assistance. Yet, we assert that these residual intensities are indeed coming from water molecules that reside in a combination of ion pairing environments within the 1ˢᵗ and 2ⁿᵈ hydration shells, that is, the water molecules immediately hydrating the Fe(III) ions and mediating the cation and anion interactions.

Ion-pairing distributions in ferric nitrate vs. chloride solutions. To better understand the effect of the presence of the diverse ion-pairing speciation present in the ferric solutions, PWS over a series of concentrations are shown in Figure 4.
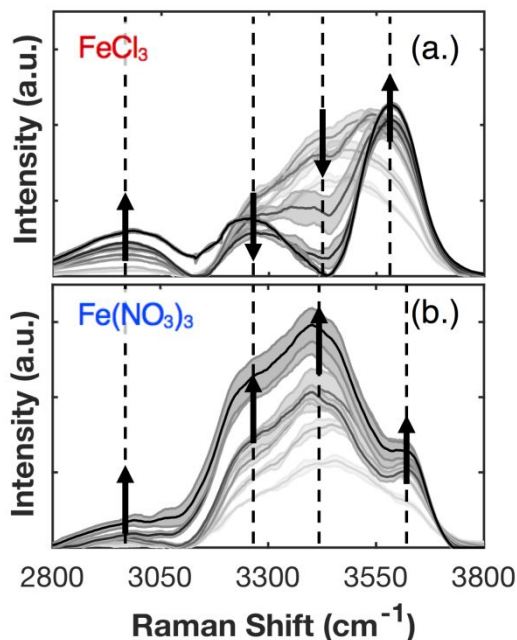
FIGURE 4 HERE

Figure 4. *Unpolarized PWS of (a.) FeCl$_3$ and (b.) Fe(NO$_3$)$_3$ with acid-removed (acid as 'solvent') over a concentration series from 0.05 to 0.6 m (light to dark grey). Arrows indicate increasing concentration.*

Figure 4 shows the PWS for the ferric chloride (Figure 4a) and ferric nitrate (Figure 4b) solutions with the relative acid chosen as the 'solvent' over a concentration range from 0.05m to 0.6m. The ferric nitrate PWS peak shape exhibits increasing intensity with increasing concentration, while the ferric chloride peak shape evolves with changing concentration. The increasing ferric nitrate bands indicate growing dissimilarity between the hydration shell of the ferric nitrate species compared to the nitric acid. This growth is attributed to a growing dissimilarity of hydrating waters around the nitrate anion, ferric ion, and ion pairs present that are different from nitric acid.

In contrast, the ferric chloride 3440 cm^{-1} PWS band of Figure 4a decreases with increasing concentration, indicating a qualitative reduction in response from the water molecules hydrating

the free chloride, similar to an HCl solution. This can be attributed to increased chloride coordination with the hexaaquo ferric ions, $[FeCl]^{2+}$ or $[FeCl_2]^+$ species. The strong increase of the 3600 cm^{-1} band in the ferric chloride PWS is attributed to the increase in concentration of weakly-hydrogen bonded water molecules that hydrate the ferric chloride species.

Distinguishing the spectral contributions of hydrating waters around the metal center vs. the nitrate anion and the chloride anion is difficult, however increasing intensity of the peak present in the weakly hydrogen bonding region (~3600 cm^{-1}) suggests an increasing abundance of solvent shared and separated ion pairs. Yet the decrease and then increased intensity with increasing frequency found in the FeCl$_3$ spectra with concentration are striking and indicative of distinct changes in hydration environments. The FeCl$_3$ PWS spectral changes are thus strongly suggestive of a combination of changing distributions of (1) Fe(III) species hydration, and (2) water-mediated ion pairing (solvent shared and separated ion pairs). We do note that both sets of spectra (Figures 4a and 4b) show a substantial increase in the 3600 cm^{-1} band with concentration, consistent with assignment to solvent shared and separated ion pair water molecules at increasing numbers.

To further explore the hydrating environments, symmetry of the collective hydration environment was exposed by independently examining the symmetric polarized (isotropic) and asymmetric polarized (anisotropic) response through the PWS. Figure 5 shows the percent isotropic response calculated via the integrated area of the anisotropic and isotropic PWS.
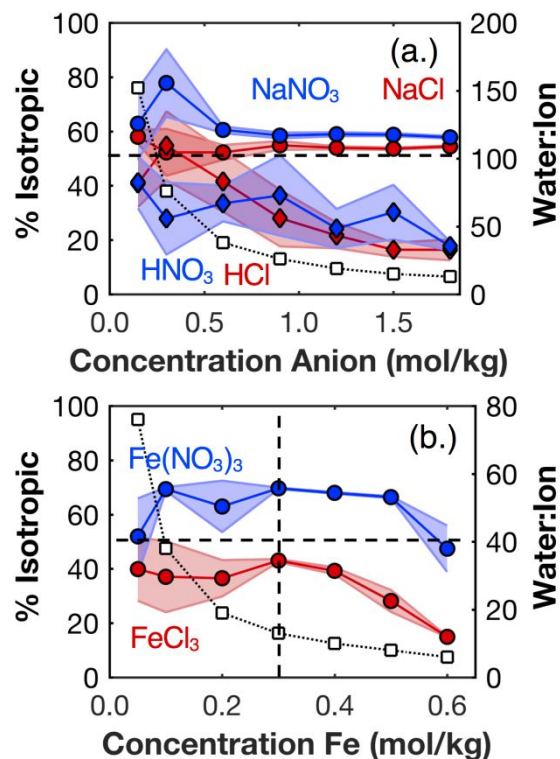
 FIGURE 5 HERE

Figure 5: Integrated area of the PWS reported as % isotropic for (a.) the salts (circles) and acids (diamonds) with water as the solvent and (b.) the ferric chloride (red circles) and nitrate (blue circles) solutions with the acid as 'solvent' vs. concentration. The ratio of the number of water molecules to each dissociated ion is shown on the right axis (open squares). Nitrate salts and acids are shown in blue and chloride salts and acids in red.

Figure 5a shows the differences between the isotropic behavior of hydrating water molecules of the salt and acid solutions versus concentration. Notably, the salts show a predominantly even distribution of a symmetric and asymmetric hydrogen bonding environment over all concentrations, while the acids increase in asymmetry with increasing concentration (where the asymmetric environment is taken as lower than 50% Isotropic). The increasing asymmetry of the acids is most likely due to the formation of Zundel and Eigen cations. Both ferric salts are inherently acidic due to hydrolysis; however, the solvating hydrogen bonding environment is

predominantly symmetric for ferric nitrate and yet predominantly asymmetric for ferric chloride

(Figure 5b). A change to the relative symmetry is observed at ~ 0.3 m for the ferric chloride

solutions. For a fully dissociated solution, this correlates to the total number of water molecules in

the first and second solvation shell of the chloride anion.[19, 20] In addition this is also a region of

considerable change to the speciation of the ferric chloride solutions as the [FeCl$_3$] concentration

becomes more abundant than [Fe(H$_2$O)$_6$]$^{3+}$ (Figure 1a). The ferric nitrate solutions also exhibit an

increase in asymmetry, though at the higher concentration of ~0.6 m, correlating to the expected

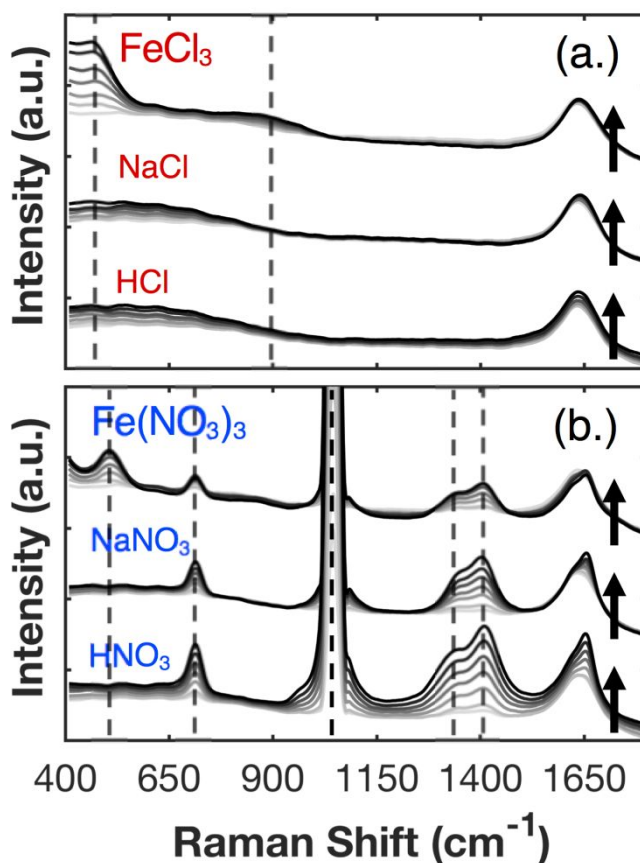formation of the ferric nitrate complex (Figure 1b).

FIGURE 6 HERE

Figure 6: *Unpolarized lower frequency Raman spectra of (a.) FeCl₃, NaCl, and HCl solutions and (b.) Fe(NO₃)₃ nitrate, NaNO₃, and HNO₃ solutions from 0.05 to 0.6 m. Arrows indicate direction of increasing concentration.*

Figure 6 shows the unpolarized lower frequency Raman spectra of the $FeCl_3$ and $Fe(NO_3)_3$ solutions over a concentration range from 0.05 to 0.6 m. The increase of the peak at ~470 cm^{-1} in the $FeCl_3$ and $Fe(NO_3)_3$ solutions is indicative of an increase of the hydrated Fe(III) species as the band is attributed to the Fe-O stretch of Fe(III) with hydrolyzed and hydrating water molecules.[22, 23, 26] Increasing the concentration results in red-shifting of the Fe-O peak in both ferric chloride and ferric nitrate solutions and is suggestive of a weakening of the Fe-O bond. Although the lower frequency broadening of the $FeCl_3$ solution spectra is due to hydrated FeClx species as well.[22] Referring to Figure 1, the fraction of hydrolyzed species decreases with increasing concentration yet there are sufficient water molecules to hydrate the ions, barely. At the higher concentrations studied, a ratio of 6 water molecules per ion is estimated at 0.6 m (Table S1 in Supporting Information). The hydration environment is thus limited to the 1st hydration shell at the higher concentrations studied here. Yet, contact ion pairs ($Fe-O_2NO$) for the ferric nitrate solutions are mostly ruled out at the concentrations studied due to lack of additional splitting evidence of the higher frequency nitrate band (~ 1300-1430 cm^{-1}), as has been observed in other nitrate –salt solutions with divalent cations, and in ferric salt melts. [23, 86 87] This is then consistent with changes in the PWS discussed above to be attributed to an increasing abundance of water-mediated ion pairs in the nitrate solutions (no direct binding by the nitrate to the Fe(III)). In the $FeCl_3$ solutions, however, the 470 cm^{-1} band broadens to below 400 cm^{-1} (limit of our spectra), consistent with both Fe-O and hydrated Fe-Cl complexation.

Conclusions

Solutions of ferric nitrate and ferric chloride were examined using polarized Raman spectroscopy and MCR-ALS analysis. The acid vs salt contributions to the Raman spectra from $FeCl_3$ and $Fe(NO_3)_3$ aqueous solution as exposed through detailed analysis is striking. We have observed using several different methods that the hydration environment and symmetry around the Fe(III) centers in ferric chloride solutions are more similar to HCl compared to ferric nitrate which shows similarity towards $NaNO_3$, despite the increased acidity in the ferric nitrate solutions (Table S2, ~ 0.2 pH units lower in the range of 0.1 to 0.6 molal). The deconvoluted hydration spectral signature informs on the water molecules taking part in water mediated ion pairing and the hydration of Fe(III) ions. We show a hydration spectral signature from the acid-removed and salt-removed spectra that is consistent with solvent shared and solvent separated ion pairs in the ferric chloride and ferric nitrate solutions. Specifically, the PWS spectra were distinctly different between the nitrate and the chloride salt of Fe(III). These results also show that anion dependent complexation is governing the hydration structure and symmetry in Fe(III) solutions.

Conflicts of Interest

There are no conflicts to declare.

Acknowledgements

Supporting Information

Details of the MCR-ALS method, average formation constants of the ferric complexes from the literature, supplemental solution properties, and vibrational and electronic spectra.

Author Information

Corresponding Author

allen@chemistry.ohio-state.edu

References

1.   J. Wadsworth and C. S. Cockell, *Scientific Reports*, 2017, **7**, 1-8.

2.   Y. Wang, M. A. Chan and E. Merino, *Scientific Reports*, 2015, **5**, 1-15.

3.   P. N. Sedwick, E. R. Sholkovitz and T. M. Church, *Geochemistry, Geophysics, Geosystems*, 2007, **8**, 1-21.

4.   Y. Takahashi, T. Furukawa, Y. Kanai, M. Uematsu, G. Zheng and M. A. Marcus, *Atmospheric Chemistry and Physics*, 2013, **13**, 7695-7710.

5.   T. D. Jickells, *Science*, 2005, **308**, 67-71.

6.   H. Matsui, N. M. Mahowald, N. Moteki, D. S. Hamilton, S. Ohata, A. Yoshida, M. Koike, R. A. Scanza and M. G. Flanner, *Nature Communications*, 2018, **9**, 1-10.

7.   M. D. Lind, *Journal of Chemical Physics*, 1967, **47**, 990-993.

8.   J. T. Szymański, *Acta Crystallographica Section B Structural Crystallography and Crystal Chemistry*, 1979, **35**, 1958-1963.

9.   N. J. Hair and J. K. Beattie, *Inorganic Chemistry*, 1977, **16**, 245-250.

10.   H. Schmidt, A. Asztalos, F. Bok and W. Voigt, *Acta Crystallographica Section C Crystal Structure Communications*, 2012, **68**, i29-i33.

11.   D. L. Wertz and M. L. Steele, *Inorganic Chemistry*, 1980, **19**, 1652-1656.

12.   G. Giubileo, M. Magini, G. Licheri, G. Paschina, G. Piccaluga and G. Pinna, *Inorganic Chemistry*, 1983, **22**, 1001-1002.

13.   T. K. Sham, J. B. Hastings and M. L. Perlman, *Journal of the American Chemical Society*, 1980, **102**, 5904-5906.

14.   I. Persson, *Journal of Solution Chemistry*, 2018, **47**, 797-805.

15.   G. J. Herdman and P. S. Salmon, *Journal of the American Chemical Society*, 1991, **113**, 2930-2939.

16.   G. J. Herdman and G. W. Neilson, *Journal of Physics: Condensed Matter*, 1992, **4**, 649-653.

17.   G. J. Herdman and G. W. Neilson, *Journal of Physics: Condensed Matter*, 1992, **4**, 627-638.

18.   L. Soderholm, S. Skanthakumar and R. E. Wilson, *Journal of Physical Chemistry A*, 2009, **113**, 6391-6397.

19.   R. Mancinelli, A. Botti, F. Bruni, M. A. Ricci and A. K. Soper, *Journal of Physical Chemistry B*, 2007, **111**, 13570-13577.

20.   M. Antalek, E. Pace, B. Hedman, K. O. Hodgson, G. Chillemi, M. Benfatto, R. Sarangi and P. Frank, *Journal of Chemical Physics*, 2016, **145**, 1-15.

21.   A. L. Marston and S. F. Bush, *Appl Spectrosc*, 1972, **26**, 579-584.

22.   S. K. Sharma, *Journal of Chemical Physics*, 1974, **60**, 1368-1375.

23.   S. K. Sharma, *Journal of Chemical Physics*, 1974, **61**, 1748-1754.

24.   S. K. Sharma, *Journal of Non-Crystalline Solids*, 1974, **15**, 83-95.

25.   S. K. Sharma, V. N. Sehgal, H. L. Bami and S. D. Sharma, *Journal of Inorganic and Nuclear Chemistry*, 1975, **37**, 2417-2419.

26.   S. K. Sharma, *Journal of Inorganic and Nuclear Chemistry*, 1973, **35**, 3831-3836.

27.   L. Ceraulo, S. Fanara, A. Ruggirello and V. T. Liveri, *J Clust Sci*, 2007, **18**, 883-895.

28.   W. G. Kong, A. Wang, J. J. Freeman and P. Sobron, *J Raman Spectrosc*, 2011, **42**, 1120-1129.

29.   F. Bohm, V. Sharma, G. Schwaab and M. Havenith, *Phys Chem Chem Phys*, 2015, **17**, 19582-19591.

30.   M. J. DiTucci, F. Böhm, G. Schwaab, E. R. Williams and M. Havenith, *Phys Chem Chem Phys*, 2017, **19**, 7297-7306.

31.   A. Eriksson, O. Kristiansson and J. Lindgren, *Journal of Molecular Structure*, 1984, **114**, 455-458.

32.   O. Kristiansson, J. Lindgren and J. De Villepin, *Journal of Physical Chemistry*, 1988, **92**, 2680-2685.

33.   D. Jamróz, M. Wójcik, J. Lindgren and J. Stangret, *Journal of Physical Chemistry B*, 1997, **101**, 6758-6762.

34.   J. Stangret and T. Gampe, *Journal of Physical Chemistry A*, 2002, **106**, 5393-5402.

35.   C. A. Daly, L. M. Streacker, Y. Sun, S. R. Pattenaude, A. A. Hassanali, P. B. Petersen, S. A. Corcelli and D. Ben-Amotz, *Journal of Physical Chemistry Letters*, 2017, **8**, 5246-5252.

36.   P. Perera, M. Wyche, Y. Loethen and D. Ben-Amotz, *Journal of the American Chemical Society*, 2008, **130**, 4576-4577.

37.   P. N. Perera, B. Browder and D. Ben-Amotz, *Journal of Physical Chemistry B*, 2009, **113**, 1805-1809.

38.   Y. Sun and P. B. Petersen, *Journal of Physical Chemistry Letters*, 2017, **8**, 611-614.

39.   J. W. Schultz and D. F. Hornig, *Journal of Physical Chemistry*, 1961, **65**, 2131-2138.

40.   W. F. Murphy and H. J. Bernstein, *Journal of Physical Chemistry*, 1972, **76**, 1147-1152.

41.   G. E. Walrafen, *Structure of water and aqueous solutions: Proceedings of the International Symposium held at Marburg in July 1973*, Verlag Chemie ; Physik-Verlag, Weinheim (Bergstr.), 1974.

42.   J. R. Scherer, S. Kint and G. F. Bailey, *Journal of Molecular Spectroscopy*, 1971, **39**, 146-148.

43.   J. Jaumot, R. Gargallo, A. de Juan and R. Tauler, *Chemometrics and Intelligent Laboratory Systems*, 2005, **76**, 101-110.

44.   J. Jaumot, A. de Juan and R. Tauler, *Chemometrics and Intelligent Laboratory Systems*, 2015, **140**, 1-12.

45.   C. F. Baes and R. E. Mesmer, *The Hydrolysis of Cations*, John Wiley & Sons, Inc, New York, NY, 1976.

46.   I. Diakonov, Université Paul Sabatier 1995.

47.   X. Liu and F. J. Millero, *Geochimica et Cosmochimica Acta*, 1999, **63**, 3487-3497.

48.   A. Stefánsson, *Environmental Science & Technology*, 2007, **41**, 6117-6123.

49.   M. Zhu, B. W. Puls, C. Frandsen, J. D. Kubicki, H. Zhang and G. A. Waychunas, *Inorganic Chemistry*, 2013, **52**, 6788-6797.

50.   K. S. Murray, *Coordination Chemistry Reviews*, 1974, **12**, 1-35.

51.   R. Seidel, K. Kraffert, A. Kabelitz, M. N. Pohl, R. Kraehnert, F. Emmerling and B. Winter, *Phys Chem Chem Phys*, 2017, **19**, 32226-32234.

52.   J. Baumgartner and D. Faivre, *Earth-Sci Rev*, 2015, **150**, 520-530.

53.   W. Liu, B. Etschmann, J. Brugger, L. Spiccia, G. Foran and B. McInnes, *Chemical Geology*, 2006, **231**, 326-349.

54.   G. A. Gamlen and D. O. Jordan, *Journal of the Chemical Society (Resumed)*, 1953, **0**, 1435-1443.

55.   E. Rabinowitch and W. H. Stockmayer, *Journal of the American Chemical Society*, 1942, **64**, 335-347.

56.   B. R. Tagirov, I. I. Diakonov, O. A. Devina and A. V. Zotov, *Chemical Geology*, 2000, **162**, 193-219.

57.   T. Sekine and T. Tetsuka, *Bulletin of the Chemical Society of Japan*, 1972, **45**, 1620-1625.

58.   M. Biruš, Z. Bradić, N. Kujundžić and M. Pribanic, *Inorganica Chimica Acta*, 1981, **56**, L43-L44.

59.   D. F. C. Morris and A. R. Wilson, *Journal of Inorganic and Nuclear Chemistry*, 1969, **31**, 1532-1536.

60.   Y. Belaustegi, M. A. Olazabal and J. M. Madariaga, *Fluid Phase Equilibria*, 1999, **155**, 21-31.

61.   K. W. Sykes, *Journal of the Chemical Society (Resumed)*, 1952, **0**, 124-129.

62.   B. N. Mattoo, *Zeitschrift für Physikalische Chemie*, 1959, **19**, 156-167.

63.   R. A. Horne, B. R. Myers and G. R. Frysinger, *Inorganic Chemistry*, 1964, **3**, 452-454.

64.   J. A. Ibers and N. Davidson, *Journal of the American Chemical Society*, 1951, **73**, 476-478.

65.   K. Murata and D. E. Irish, *Spectrochimica Acta Part A: Molecular Spectroscopy*, 1988, **44**, 739-743.

66.   M. Magini and T. Radnai, *Journal of Chemical Physics*, 1979, **71**, 4255-4262.

67.   M. Magini, *Journal of Chemical Physics*, 1982, **76**, 1111-1115.

68.   Y. X. Chen, H. I. Okur, N. Gomopoulos, C. Macias-Romero, P. S. Cremer, P. B. Petersen, G. Tocci, D. M. Wilkins, C. W. Liang, M. Ceriotti and S. Roke, *Sci Adv*, 2016, **2**.

69.   Y. Chen, H. I. Okur, C. Liang and S. Roke, *Phys Chem Chem Phys*, 2017, **19**, 24678-24688.

70.   M. Ahmed, A. K. Singh, J. A. Mondal and S. K. Sarkar, *Journal of Physical Chemistry B*, 2013, **117**, 9728-9733.

71.   J. D. Smith, R. J. Saykally and P. L. Geissler, *Journal of the American Chemical Society*, 2007, **129**, 13847-13856.

72.   Y. Marcus and G. Hefter, *Chemical Reviews*, 2006, **106**, 4585-4621.

73.   R. A. Robinson, *Journal of the American Chemical Society*, 1935, **57**, 1165-1168.

74.   J. N. Pearce and H. Hopson, *Journal of Physical Chemistry*, 1937, **41**, 535-538.

75.   P. Olynyk and A. R. Gordon, *Journal of the American Chemical Society*, 1943, **65**, 224-226.

76.   J. N. Pearce and A. F. Nelson, *Journal of the American Chemical Society*, 1932, **54**, 3544-3555.

77.   W. J. Hamer and Y. C. Wu, *Journal of Physical and Chemical Reference Data*, 1972, **1**, 1047-1100.

78.   R. Haas, K. H. Dücker and H. A. Küppers, *Berichte der Bunsengesellschaft für physikalische Chemie*, 1965, **69**, 97-109.

79.   W. Davis and H. J. De Bruin, *Journal of Inorganic and Nuclear Chemistry*, 1964, **26**, 1069-1083.

80.   R. Flatt and F. Benguerel, *Helvetica Chimica Acta*, 1962, **45**, 1765-1772.

81.   W. F. K. Wynne-Jones, *Journal of the Chemical Society*, 1930, **0**, 1064-1071.

82.   R. A. Robinson, *Transactions of the Faraday Society*, 1936, **32**, 743-744.

83.   H. J. E. Dobson and I. Masson, *Journal of the Chemical Society, Transactions*, 1924, **125**, 668-676.

84.   M. Thamer, L. De Marco, K. Ramasesha, A. Mandal and A. Tokmakoff, *Science*, 2015, **350**, 78-82.

85.   J. Kim, U. W. Schmitt, J. A. Gruetzmacher, G. A. Voth and N. E. Scherer, *Journal of Chemical Physics*, 2002, **116**, 737-746.

86.   M. Xu, J. P. Larentzos, M. Roshdy, L. J. Criscenti and H. C. Allen, *Phys Chem Chem Phys*, 2008, **10**, 4793-4801.

87.   N. H. C. Lewis, J. A. Fournier, W. B. Carpenter and A. Tokmakoff, *The Journal of Physical Chemistry B*, 2018, **123**, 225-238.

Graphical Abstract

Ferric ion hydration differences are governed by ion pair formation uniquely affected by anion identity.